View Article Online / Journal Homepage / Table of Contents for this issue
Dynamic Article Links

Lab on a Chip

Cite this: *Lab Chip*, 2012, **12**, 5138–5141

www.rsc.org/loc

TECHNICAL INNOVATION

Published on 19 September 2012. Downloaded by UNIVERSITY OF CINCINNATI on 08/01/2014 20:37:02.

Deterministic splitting of fluid volumes in electrowetting microfluidics†

Ananda Banerjee, Yuguang Liu, Jason Heikenfeld and Ian Papautsky*

Received 27th June 2012, Accepted 19th September 2012
DOI: 10.1039/c2lc40723j

Conventional droplet generation approaches in digital microfluidics show ~10% variation in droplet volumes and are restricted to creating only small volumes. In this work, we demonstrate a new approach for splitting sample volumes precisely by gradually ramping down voltage, in place of abruptly switching off electrodes. This allows us to eliminate hydrodynamic instabilities responsible for variations in droplet volume. A simple visual method was developed for measuring sample volumes created on-chip. Our results show that generating and measuring arbitrary sample volumes accurately, with $< 1\%$ variation, is possible in electrowetting devices. The approach can be easily extended to existing digital microfluidic systems, and can potentially improve performance of applications requiring precise sample metering, such as immunoassays or DNA amplification.

Introduction

Electrowetting microfluidic devices have emerged in recent years, offering advantages of programmable functionality.[1–4] Programmed manipulation of droplets using electrowetting is commonly referred to as digital microfluidics and has been used to demonstrate a number of lab-on-a-chip applications.[5–11] Using electrowetting, we recently demonstrated continuous microfluidic channels that are reconfigurable and can sustain pressure driven flows.[12] This would enable programmable electrowetting devices to take advantage of a vast library of existing microfluidic applications.[13]

In digital microfluidics, most applications (*e.g.*, immunoassays,[14] DNA amplification,[15,16] cell-based screening[17]) are highly sensitive to variations in sample volume,[18] yet droplet generation approaches show a ~10% variability. Splitting a droplet typically involves abrupt de-activation of an energized electrode and thus de-wetting migration of fluid to the adjoining energized electrodes. Variations in the generated droplet volume have been attributed to hydrodynamic instabilities arising in the splitting region and decrease in volume of the source reservoir.[10] A more precise method of volume control has recently been reported using capacitive feedback control.[19] However, this approach requires additional signal processing and may not be readily adaptable to electrowetting channels.

In this work, we demonstrate a simple approach for deterministic splitting of liquids with high degree of accuracy that does not require feedback control. In our approach, the hydrodynamic instabilities in the splitting region are minimized by slowly (> 1 s) ramping down splitting electrode potential. A technique for observing sample volumes was developed for measuring accuracy of the splitting mechanism. Sample volumes generated by controlling potential at the splitting region yielded sample volumes with $< 1\%$ variation.

Experimental

For all experiments, we used our recently-reported platform based on programmable virtual microchannels.[12,13] It is analogous to the two-plate electrowetting manipulation of droplets, but is capable of handling larger fluid volumes and allowing pressure driven flows. Our specific device for this work consisted of three 500 μm wide electrodes in the shape of a microchannel, with the shortest being a 3-mm long splitting electrode in the middle (Fig. 1a). Channel electrodes adjacent to the splitting electrode were each 11 mm in length and connected the inlet and outlet ports. A visual length marker was patterned adjacent to the splitting electrode for measuring fluid position during splitting. In addition, a width marker consisted of parallel 10 μm wide lines and 10 μm spacing, was patterned next to the channel electrodes for observing changes in volume (bulging) during the splitting process. The splitting electrode was electrified through two variable 1 MΩ resistors so that applied potential could be precisely controlled by varying a second resistor in series (Fig. 1b). The applied potential was monitored with a voltmeter across the second resistor. A transparent conductive top plate (100 nm ITO over glass) provided electrical ground, and contained drilled inlet and outlet ports. The height of the channel was defined by using a 100 μm thick spacer layer between the top and bottom substrates.

We fabricated devices on a 50 mm × 50 mm glass substrate. The metal electrodes (100 nm Au on 20 nm Ti) were photolithographically patterned on it with electrical contacts at the substrate edge. The metal electrodes were insulated by a 1 μm thick layer of Parylene-C (Specialty Coating Systems). The

School of Electronic and Computing Systems, University of Cincinnati, Cincinnati, OH, 45221, USA. E-mail: ian.papautsky@uc.edu; Tel: +1 (513) 556-2347

† Electronic supplementary information (ESI) available. See DOI: 10.1039/c2lc40723j

This journal is © The Royal Society of Chemistry 2012

Published on 19 September 2012. Downloaded by UNIVERSITY OF CINCINNATI on 08/01/2014 20:37:02.

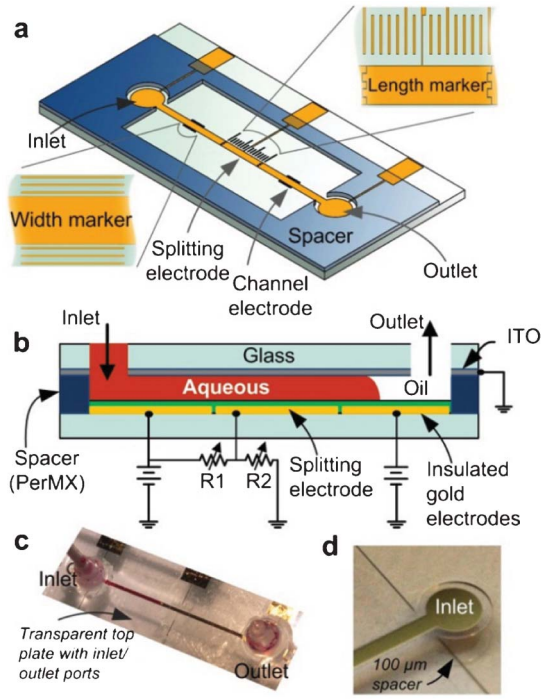


Fig. 1 (a) Electrowetting based device for demonstrating deterministic splitting and volume generation. The increase in volume (bulging) due to fluid redistribution can be measured using the included width markers. Length markers along the splitting electrode can be used for observing the position of splitting. (b) Cross-section of electrowetting based device. (c) Formation of 500 μm wide, 25 mm long microfluidic channel. (d) Magnified image of the inlet/outlet reservoir patterned in the spacer layer.

spacer layer defining channel height was patterned around the edges of the device using a negative photoresist (Dupont Permx 3050). The spacer layer also formed the physical boundaries of the reservoirs at the inlet and outlet ports (Fig. 1d). Both the top and bottom substrates were coated with a thin (50 nm) layer hydrophobic fluoropolymer (Cytonix Fluoropel 1601 v) to make surfaces hydrophobic and ensure that the aqueous fluid has a contact angle (Young's angle) of $\sim 180^\circ$ in oil. The top and bottom substrates were bonded together using an UV-curable epoxy (Dymax), ensuring that the device was sealed on all sides except at the inlet and outlet ports. Ferrules were epoxy-bonded to the inlet/outlet ports in the top plate to connect tubing for the conducting liquid sample (red) and ambient oil (OS-30, Dow Corning). The cavity of the device was filled with oil before the aqueous sample was introduced. We used 100 mM sodium phosphate solution mixed with red aqueous pigment dispersion (Sun Chemical) as the aqueous conducting fluid (~ 72 mN m^{-1}).

A virtual microfluidic channel was formed over all three voltage-activated electrodes with the introduction of the aqueous sample at the inlet (Fig. 1c). Excess oil left the cavity of the device through the outlet. As we characterized in our earlier work, saturation potential for this aqueous fluid is < 70 V with the saturation contact angle of $\sim 60^\circ$.[12] A continuous source of fluid allowed us to overcome possible issues associated with variation in reservoir volume.[10] The inlet and outlet reservoirs were completely filled with equal fluid levels to ensure symmetry, before splitting.

Results and discussion

Laplace pressure across the aqueous-oil interface is as a function of horizontal (R_h) and vertical (R_v) radii of curvatures of the meniscus and the interfacial tension γ_{ci} between the conducting fluid and the insulating oil.

$$\Delta p = \gamma_{ci}(1/R_h + 1/R_v) \quad (1)$$

Our previous work[12] shows that the sidewall vertical radius of curvature (R_s) differs from the front of the meniscus. The R_s and the bottom contact angle at the sidewalls (θ_s) can be obtained by equating the Laplace pressures at the front of the advancing meniscus with the Laplace pressure at the sidewalls[12]

$$R_s = \frac{hw}{2h - w(\cos\theta_0 + \cos\theta_{sat})} \quad (2)$$

$$\theta_s = \cos^{-1}\left(\cos\theta_{sat} - \frac{2h}{w}\right) \quad (3)$$

where h is the height of the channel, w is the width of the channel, θ_0 is the contact angle when no voltage is applied, θ_{sat} is the saturated contact angle at an applied voltage such that increasing voltage does not change this value. For our system, $\theta_0 = 180^\circ$ and $\theta_{sat} = 60^\circ$.[12] The channel dimensions h (spacer thickness) and w (electrode width) are 100 μm and 500 μm respectively. For our device at equilibrium, the sidewall radius of curvature is $R_s \sim 111$ μm and bottom contact angle at the sidewalls is $\theta_s \sim 84^\circ$. At equilibrium, the area of the channel cross-section A is given by (refer to ESI† for detailed derivation):

$$A = hw - R_s \sin\theta_s(h + R_s) + \frac{\theta_s}{180}\pi R_s^2 \quad (4)$$

When voltage at the center-splitting electrode is turned off (or reduced), the fluid over the splitting region de-wets as compared to the adjacent energized electrodes. Fluid from the splitting region migrates to the adjoining electrowetted regions, causing the microchannel to shrink over the splitting electrode, with bulging over the adjacent channel electrodes from their original equilibrium shape. This is schematically shown in Fig. 2. This increase in the cross-section of fluid segments is accompanied by a reduction in the sidewall radius of curvature R_s, and a consequent increase in the apparent sidewall contact angle θ_s at the bottom (Fig. 3a).

Redistribution of volume from the splitting region to the adjoining voltage-activated regions was examined by observing the change in the sidewall bulge. When seen from the top, the bulge in the sidewalls appears to form a uniformly advancing front, as illustrated in Fig. 2. The projection of the bulge, w_p can be related to the radius of curvature of the sidewalls, R_s and the sidewall contact angle of the at the bottom, θ_s by the following relation:

$$w_p = 2R_s \sin^2\left(\frac{\theta_s - 90}{2}\right) \quad (5)$$

Changes in projection length with increasing bottom contact angle (bulging) are illustrated in Fig. 3. The precise volume of

Published on 19 September 2012. Downloaded by UNIVERSITY OF CINCINNATI on 08/01/2014 20:37:02.

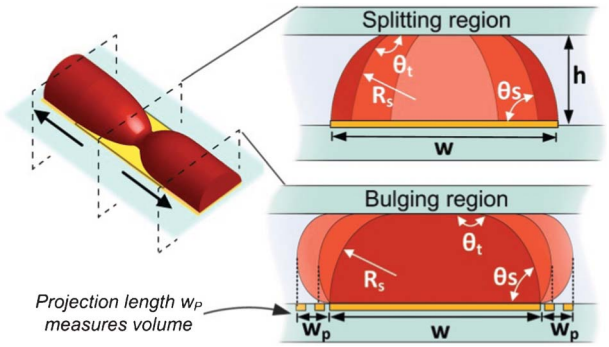


Fig. 2 Fluid redistribution during ramped splitting causes microchannel in the splitting region to shrink and the adjacent regions to bulge from their original equilibrium shape. Equilibrium cross-section is dark red, with lighter shades indicating splitting progression. The projection of the bulged sidewall can be viewed from top and used to calculate volume.

fluid segments of known length created by the process of splitting can be calculated by measuring the projection length experimentally and finding the corresponding value of the bottom contact angle and the associated area of cross-section from the graph (Fig. 3). The final volume of the channel is the product of the length of the channel and its cross-section. The process of visual volume measurement was aided by the width markers lining the channel electrodes. This method of volume calculation is generally applicable to any electrowetting on dielectric based system for known values of θ_0 and θ_{sat}.

Under equilibrium conditions, migration of fluid to the adjoining electrowetted segments should be governed by the maintenance of uniform Laplace pressures at all regions of the oil–water interface. This implies that fluid migration to either side of the splitting region would be determined by the ability of the adjoining electrowetted segments to accommodate the excess volume through bulging of sidewalls. This is consistent with the mechanisms of droplet splitting described in literature.[10,20] The lengths of the electrowetted segments on either side of the splitting region ultimately determine the amount of volume that can be accommodated. If the voltage at the splitting electrode is switched off abruptly, the fluid volume occupying this region becomes hydrodynamically-unstable without any confining forces to hold it in place. Migration of the fluid from this region to the adjoining voltage-activated segments becomes unpredictable due to the short time during which the mass transfer occurs. The rapid mass transport causes local perturbations to develop on either side of the splitting region, leading to local changes in Laplace pressure and the resulting unpredictable nature of the fluid distribution.

A more deterministic approach for dispensing electrowetted fluid volumes must account for the time required for mass-transfer from the splitting region to the adjoining segments. Fluid migration from the splitting region to the adjacently-located existing fluid can be controlled in a more predictable manner if voltage applied at the splitting electrode is gradually reduced. We assumed that for longer splitting lengths and wider channels mass transfer would take longer. This would allow time for mass transfer from the splitting region to proceed under near-equilibrium conditions. Excess fluid accommodated at the electrowetted regions on either side of the splitting electrode causes equal bulging, such that the Laplace pressure is the same at all regions along the aqueous-oil interface. Simulations were conducted in CFD-ACE+ (ESI†) to predict the optimized time necessary for mass transfer from the splitting region and the slope of the ramp. It was found that for a splitting region length of 200 μm in a 100 μm wide channel, the minimum time required for deterministic splitting is 160 ms with a uniform ramp from 70 V to 30 V. For longer splitting lengths and wider channels mass transfer would take longer and hence slower ramps would be necessary.

To test that gradually reducing voltage at the splitting region leads to deterministic splitting, we conducted two sets of experiments. All experiments involved splitting a 25 mm long fluid segment at the center, over a splitting electrode 3 mm in length. The volume of the entire microchannel was 1.12 μL. In the first set of experiments, we gradually ramped down the voltage applied to the splitting electrode by changing the resistance of the network through which the splitting electrode was connected. In the latter set, the same experiment was repeated by abruptly grounding the splitting electrode. The volume of the split segments on both sides of the splitting region was observed in both cases and calculated by measuring the projection length of the bulge on either side of the splitting region as described previously.

When voltage was abruptly turned off at the splitting electrode, we observed that the fluid migration to either side of the splitting region was unpredictable. The projection lengths on both sides of the splitting region were unequal. A representative

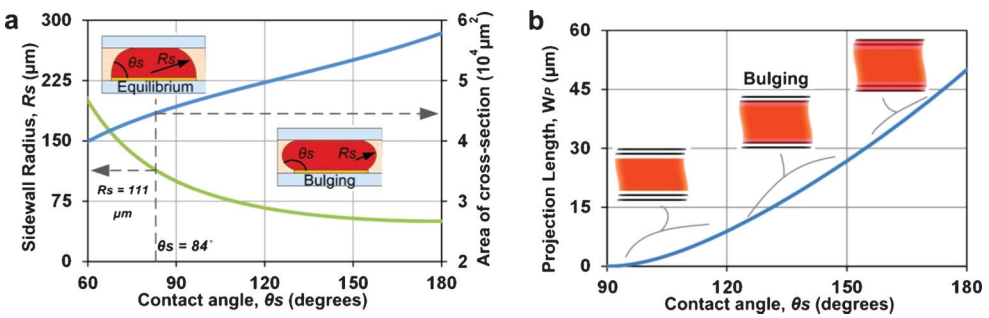


Fig. 3 Microchannel sidewalls bulge to accommodate migrating fluid from the splitting region. (a) Plot shows the decrease in the sidewall radius of curvature and the increase in area of cross-section with increasing bottom contact angle θ_s. (b) The projection of the bulged sidewalls seen from the top can be used as measure of the area of cross-section of the microchannel. The projection length w_p increases with increase in bulging. Each value of w_p corresponds to a particular value of θ_s and an associated area of cross-section.

 This journal is © The Royal Society of Chemistry 2012

Published on 19 September 2012. Downloaded by UNIVERSITY OF CINCINNATI on 08/01/2014 20:37:02.

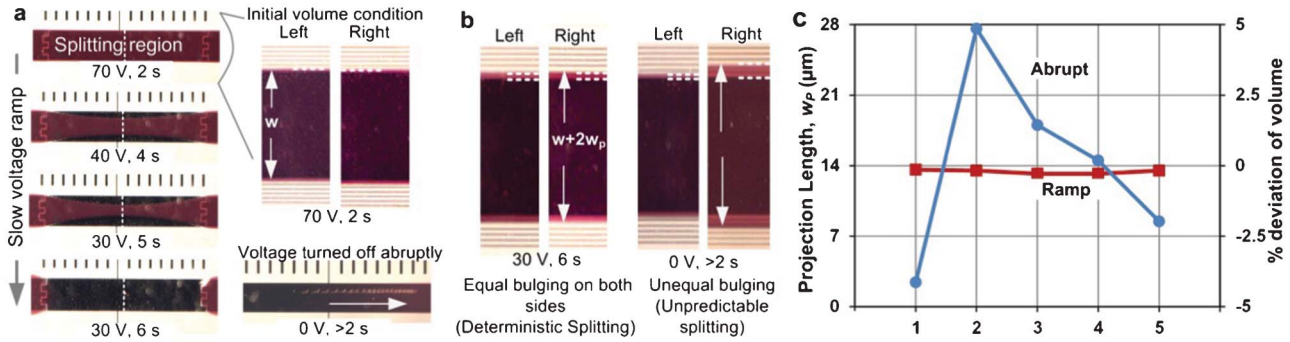


Fig. 4 (a) Experimental results showing both deterministic and unpredictable splitting at centered electrode. For the gradual voltage ramp, a symmetric radius of curvature is observed. (b) The final bulge on both sides is equal ($w_p \sim 13.5$ μm–indicated with dashed white lines) for gradually ramped splitting. Abruptly turning off voltage leads to hydrodynamic instabilities and disproportional fluid distribution, as indicated by the unequal bulging on two sides. (c) The target volume on each side was ~ 0.56 μL.

result is shown in Fig. 4, illustrating that most of the volume over the splitting region migrated to one side causing it to bulge more. The initial width of the virtual channel, w is the same as the electrode width (500 μm). We measure the projection length of the bulged channel by first obtaining the entire width of the bulged channel ($w + 2w_p$) and then subtracting the width of the channel from this. In this case, the projection length was ~ 26 μm on one side and ~ 5 μm on the other. The volume of the segment was calculated to be ~ 0.586 μL, with the volume of the other segment ~ 0.534 μL. This is a deviation of $\pm 5\%$ from the targeted volume of 0.558 μL. The standard deviation in volume was found to be 0.02 μL ($n = 5$). The accuracy of the method of measurement was confirmed by the fact that the sum of the individually-measured/calculated split volumes added up to the initial volume of the microchannel.

Gradually decreasing voltage at the splitting electrode yielded two split fluid segments of equal volume, as illustrated in Fig. 4. The splitting progressed with the formation of symmetric radii of curvature on the sidewalls over the splitting electrode. Fluid migrated to the adjoining voltage activated regions causing them to bulge. When splitting was completed, the projection length of the bulged segments was measured using the 10 μm width markers patterned on either side. The projection length was found to be ~ 13.5 μm on either side of the splitting region yielding a volume of ~ 0.558 μL on either side. The experiments were repeated 5 times and the measurements were found to be within 1% maximum variation. The standard deviation in volume was found to be 0.001 μL (n = 5). The volumes created on both sides of the splitting region were equal confirming our hypothesis.

Conclusions

The characterization of results in applications such as immunoassays depends on the concentration of analytes in droplets. Dispensing and splitting have been shown to be the main source of degradation in assay performance.[21] Feedback-based droplet dispensing systems with elaborate signal processing modules have been demonstrated with highly mono-disperse droplet characteristics.[19] In contrast, our system is simple in design and can be used to generate and manipulate arbitrary sample volumes in the form of droplets or virtual channels with similar precision. The incorporation of visual width markers provides a simple real-time monitoring system for characterizing sample volume. The concept of ramped splitting for dispensing finite sample volumes is a readily adaptable and can potentially benefit electrowetting applications requiring accurate sample dispensing.

Acknowledgements

We gratefully acknowledge support by the National Science Foundation (ECCS-1001141).

References

1 J. Berthier, *Micro-Drops and Digital Microfluidics*, William Andrew Publishing, Norwich, NY, 2008.
2 A. R. Wheeler, *Science*, 2008, **322**, 539–540.
3 S. K. Cho and H. Moon, *Biochip Journal*, 2009, **2**, 79–96.
4 S. Teh, R. Lin, L. Hung and A. P. Lee, *Lab Chip*, 2008, **8**, 198–220.
5 R. B. Fair, *Microfluid. Nanofluid.*, 2007, **3**, 245–281.
6 R. B. Fair, A. Khlystov, T. D. Tailor, V. Ivanov, R. D. Evans, V. Srinivasan, V. K. Pamula, M. G. Pollack, P. B. Griffin and J. Zhou, *IEEE Des. Test Comput.*, 2007, **24**, 10–24.
7 J. P. Urbanski, W. Thies, C. Rhodes, S. Amarasinghe and T. Thorsen, *Lab Chip*, 2006, **6**, 96–104.
8 V. Srinivasan, V. K. Pamula and R. B. Fair, *Anal. Chim. Acta*, 2004, **507**, 145–150.
9 V. Srinivasan, V. K. Pamula and R. B. Fair, *Lab Chip*, 2004, **4**, 310–315.
10 S. K. Cho, H. Moon and C. J. Kim, *J. Microelectromech. Syst.*, 2003, **12**, 70–80.
11 M. J. Jebrail and A. R. Wheeler, *Curr. Opin. Chem. Biol.*, 2010, **14**, 574–581.
12 A. Banerjee, E. Kreit, Y. Liu, J. Heikenfeld and I. Papautsky, *Lab Chip*, 2012, **12**, 758–764.
13 M. Dhindsa, J. Heikenfeld, S. Kwon, J. Park, P. D. Rack and I. Papautsky, *Lab Chip*, 2010, **10**, 832–836.
14 N. Vergauwe, D. Witters, F. Ceyssens, S. Vermeir, B. Verbruggen, R. Puers and J. Lammertyn, *J. Micromech. Microeng.*, 2011, **21.**
15 Y. -Chang, G. -Lee, F. -Huang, Y. -Chen and J. -Lin, *Biomed. Microdevices*, 2006, **8**, 215–225.
16 L. Malic, T. Veres and M. Tabrizian, *Biosens. Bioelectron.*, 2009, **24**, 2218–2224.
17 D. Bogojevic, M. D. Chamberlain, I. Barbulovic-Nad and A. R. Wheeler, *Lab Chip*, 2012, **12**, 627–634.
18 N. Vergauwe, D. Witters, Y. T. Atalay, B. Verbruggen, S. Vermeir, F. Ceyssens, R. Puers and J. Lammertyn, *Microfluid. Nanofluid.*, 2011, **11**, 25–34.
19 J. Gong and C. -Kim, *Lab Chip*, 2008, **8**, 898–906.
20 J. Berthier, P. Clementz, O. Raccurt, D. Jary, P. Claustre, C. Peponnet and Y. Fouillet, *Sens. Actuators, A*, 2006, **127**, 283–294.
21 H. Ren, R. B. Fair and M. Pollack, *Sens. Actuators, B*, 2004, **98**, 319–327.